ENVIRONMENTAL RESEARCH
LETTERS

LETTER

Plant functional type aboveground biomass change within Alaska and northwest Canada mapped using a 35-year satellite time series from 1985 to 2020

Kathleen M Orndahl[1,*], Matthew J Macander[2], Logan T Berner[1] and Scott J Goetz[1]

[1] School of Informatics, Computing and Cyber Systems, Northern Arizona University, Flagstaff, AZ 86011, United States of America
[2] ABR, Inc.—Environmental Research & Services, Fairbanks, AK 99708, United States of America
* Author to whom any correspondence should be addressed.

E-mail: kmo265@nau.edu

Keywords: plant functional type, aboveground biomass, Landsat, remote sensing, tundra, UAV, fire

Supplementary material for this article is available online

OPEN ACCESS

RECEIVED
16 May 2022

REVISED
18 October 2022

ACCEPTED FOR PUBLICATION
25 October 2022

PUBLISHED
11 November 2022

Abstract

Changes in vegetation distribution are underway in Arctic and boreal regions due to climate warming and associated fire disturbance. These changes have wide ranging downstream impacts—affecting wildlife habitat, nutrient cycling, climate feedbacks and fire regimes. It is thus critical to understand where these changes are occurring and what types of vegetation are affected, and to quantify the magnitude of the changes. In this study, we mapped live aboveground biomass for five common plant functional types (PFTs; deciduous shrubs, evergreen shrubs, forbs, graminoids and lichens) within Alaska and northwest Canada, every five years from 1985 to 2020. We employed a multi-scale approach, scaling from field harvest data and unmanned aerial vehicle-based biomass predictions to produce wall-to-wall maps based on climatological, topographic, phenological and Landsat spectral predictors. We found deciduous shrub and graminoid biomass were predicted best among PFTs. Our time-series analyses show increases in deciduous (37%) and evergreen shrub (7%) biomass, and decreases in graminoid (14%) and lichen (13%) biomass over a study area of approximately 500 000 km^2. Fire was an important driver of recent changes in the study area, with the largest changes in biomass associated with historic fire perimeters. Decreases in lichen and graminoid biomass often corresponded with increasing shrub biomass. These findings illustrate the driving trends in vegetation change within the Arctic/boreal region. Understanding these changes and the impacts they in turn will have on Arctic and boreal ecosystems will be critical to understanding the trajectory of climate change in the region.

1. Introduction

Arctic and boreal regions are warming over three times as fast as the rest of the planet [1], leading to significant changes in vegetation community composition and structure [2, 3]. These changes include expansion of deciduous shrubs and increases in plant productivity in Arctic and alpine tundra [4–11]. Although less common, localized decreases in productivity have been observed and linked with winter warming and disturbances including extreme climatic events [8, 12–15]. In boreal regions, warming has increased vegetation productivity and tree recruitment along the forest-tundra ecotone, while also increasing tree mortality from drought and wildfires [16–22]. Such changes trigger cascading effects [7, 23] that impact surface albedo [24, 25], carbon and nitrogen cycling [26–29], snow cover and water balance [25], fire regimes [30], wildlife forage and habitat [31, 32], and permafrost dynamics [27, 33–36]. Consequently, monitoring changes in vegetation is crucial for understanding and managing climate change impacts in the Arctic-boreal Zone (ABZ). Changes in vegetation during recent decades have been monitored across the ABZ using satellite remote sensing, revealing widespread greening [8, 37–39] and localized browning [8, 14] in Arctic and alpine tundra. In boreal regions, greening has

been observed primarily along the forest-tundra ecotone, whereas browning has been observed primarily along the warmest margins [21]. Studies monitoring greening and browning predominantly rely on the Normalized Difference Vegetation Index (NDVI) or other metrics of vegetation 'greenness' that broadly correlate with vegetation productivity and aboveground biomass (AGB). However, these metrics do not discriminate between plant functional types (PFTs) [40], nor account for vegetation structure. Therefore, there have been increasing efforts to map land cover types and/or fractional plant cover [41–45], as well as three dimensional vegetation structure including AGB [46, 47].

These advancements are important for several reasons. First, identifying which PFTs are expanding is important for understanding current and future vegetation and climate dynamics. For example, shrub expansion is not limited to deciduous shrubs, but also includes evergreen shrubs [48]. Discriminating between deciduous and evergreen shrub expansion is important because the implications of expansion are notably different—expansion of shorter stature evergreen shrubs is less likely to exert a positive feedback on climate warming [49]. Furthermore, increasing vegetation cover is not limited to shrubs, but can also include forbs and graminoids, especially grasses [4, 5]. Conversely, increases in PFTs such as deciduous shrubs can cause decreases in lichens and other PFTs [4, 50–53]. Since lichen are critical winter forage, this has detrimental impacts on caribou, which are in decline across much of the ABZ [50, 54]. Downstream effects of climate change such as changes in herbivory [55] and fire regimes [30, 56] also affect PFTs differentially, which highlights the importance of precisely mapping where and how PFTs are changing in a warming ABZ. Moreover, changes in vegetation do not occur solely in a two-dimensional plane. Rather, increased shrub height and density are critical aspects of shrub expansion [4–6, 57]. The AGB of individual PFTs has been mapped at local scales (mapped area 0.25 m^2–12.5 km^2) using field-based biomass harvests combined with imagery from aircraft and/or unmanned aerial vehicles (UAVs). These efforts typically utilized red-green-blue and multispectral imagery to classify scenes and then relied on either Structure from Motion or lidar data to create canopy height models and predict biomass [58–62]. At the regional scale, Landsat satellite imagery has been used with airborne lidar to map boreal tree AGB in Canada [63], and with biomass harvest data to map arctic shrub AGB across the Alaska North Slope [46]. However, there are no regional biomass maps in Alaska and northwest Canada that parse biomass by multiple PFTs.

We mapped live AGB of non-tree PFTs (AGB_{PFT}) within Alaska and northwest Canada from 1985 to 2020 using biomass harvest, UAV, and Landsat satellite datasets. Individual PFTs included deciduous shrubs, evergreen shrubs, forbs, graminoids, and lichens. This effort focused on non-forested vegetation communities, but the study area included boreal regions. In areas where trees were present, our maps represent understory biomass only. We bridged the spatial gap between field data and satellite imagery using UAV based biomass maps [43, 64, 65]. Specifically, we:

(a) Compared accuracy of AGB_{PFT} modeled using satellite predictor data when trained using field vs. UAV based estimates of AGB_{PFT}.
(b) Assessed spatial variation in AGB_{PFT} across the region.
(c) Evaluated changes in AGB_{PFT} from 1985 to 2020.
(d) Examined how fires influenced changes in AGB_{PFT} in recent decades.

2. Methods

2.1. Study area

We mapped AGB_{PFT} across approximately 500 000 km^2 in Alaska and northwest Canada, corresponding to the extended ranges of the Porcupine and Fortymile caribou herds (figure 1). These caribou herds are culturally, ecologically and economically important across our study area. Since AGB_{PFT} determines wildlife habitat and forage, mapping AGB_{PFT} across this area provides valuable insight for wildlife management. Vegetation communities in this region range from boreal forest to dense shrublands to wet tundra and lichen barrens (table S1).

2.2. Field and UAV data collection and aggregation

During the summers of 2018 and 2019, we collected field data at 44 sites across the study area (table S1, figure 1). These sites capture the range in non-forest vegetation community types that occur across the region. At each site, we harvested live AGB at five 0.25 m^2 quadrats placed at 20 m intervals along a 100 m transect oriented parallel to the topographic contour. Harvested biomass was sorted into PFTs (deciduous shrub, evergreen shrub, forb, graminoid, lichen), oven-dried to a constant weight, and weighed with a precision of 0.0001 g. We also collected UAV imagery at each of the 44 sites. This UAV imagery was subsequently used to locally map AGB_{PFT}. This mapping was done by modeling pixel-wise AGB_{PFT} from pixel-wise volume, derived from Structure from Motion based canopy height models. For additional details on field data and UAV-based mapping see Orndahl *et al* [66].

We created two training/validation datasets, one aggregated directly from field biomass harvest data ('field-based data,' $n = 266$) and one aggregated from UAV-based AGB_{PFT} maps ('UAV-based data,' $n = 427$), to assess how model performance varied based on differences in scale from training data to final map resolution. For both datasets, observations

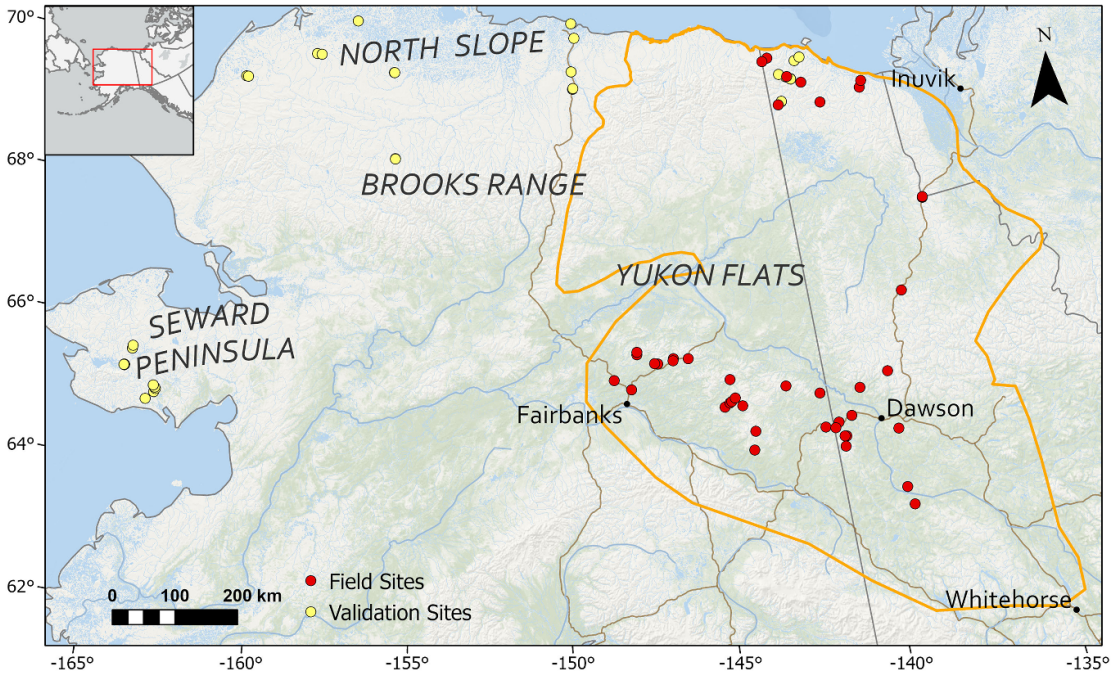

Figure 1. Map of field site locations ($n = 44$, red points), as well as validation site locations ($n = 49$, yellow points). The study area is outlined in orange.

were 30 m pixels with biomass predictions derived from either field or UAV data (figures S1 and S2). Data aggregation details are provided in supplementary text 1.

2.3. Landsat spectral predictors and environmental predictors

We processed remotely sensed predictors in Google Earth Engine (GEE) [67]. To produce time series data, we analyzed all available Landsat 4/5/7/8 Collection 1 Tier 1 surface reflectance data from April 1st to September 30th for 1984–2020. Imagery was masked to exclude clouds, cloud shadows, snow, surface water, and gaps using the quality flags provided by CFMASK [68]. We also masked pixels with Normalized Differenced Snow Index (NDSI) >0.1 to remove some water bodies and subpixel snow. We normalized Landsat 8 reflectance and NDVI to Landsat 7 following [69], and Landsat 4 and 5 NDVI to Landsat 7 [37].

After quality-screening the Landsat imagery, we generated seasonal spectral predictors using the Continuous Change Detection and Classification (CCDC) algorithm [70]. First, we applied the CCDC algorithm to model the reflectance bands, thermal band, and NDVI (table S2). Using these model fits, we generated annual synthetic reflectance values for specific seasonal percentiles. Seasonal percentiles were defined as percentiles of the snow-free season. For example, summer was represented by the day of year corresponding to the 50th percentile of snow-free days (table S3). The other indices listed in table S2 were calculated from the synthetic reflectance estimates. We also calculated the daily rate of change for each season, and the overall mean, median and amplitude (maximum minus minimum) for each band/index. This resulted in 320 seasonal spectral predictors, listed in table S3. The CCDC modeling process filled gaps caused by clouds or other interference including Landsat 7 Scan Line Corrector gaps, and produced a continuous time series for each pixel, except for temporal gaps between time segment breaks. Temporal gaps were filled by iteratively assigning spectral data from the closest available year. We supplemented spectral predictors with a suite of environmental predictors related to climate, topography, permafrost, and vegetation (table S3). These procedures for Landsat data pre-processing and derivation of seasonal spectral predictors follow recent advances in vegetation mapping [45, 70, 71].

2.4. Modeling

We modeled AGB_{PFT} as a function of the predictors in table S3. Because our predictor set was large, we employed a multi-stage approach to reduce the pool of available predictors before model fitting. First, we excluded predictors for which the standard deviation across our training data was less than 50% of the standard deviation across the full study area, as a model trained on this data would be subject to extrapolation when applied over the full study area. Then, we removed highly correlated predictors using hierarchical clustering across a range of distance thresholds. This produced a list of predictor subsets,

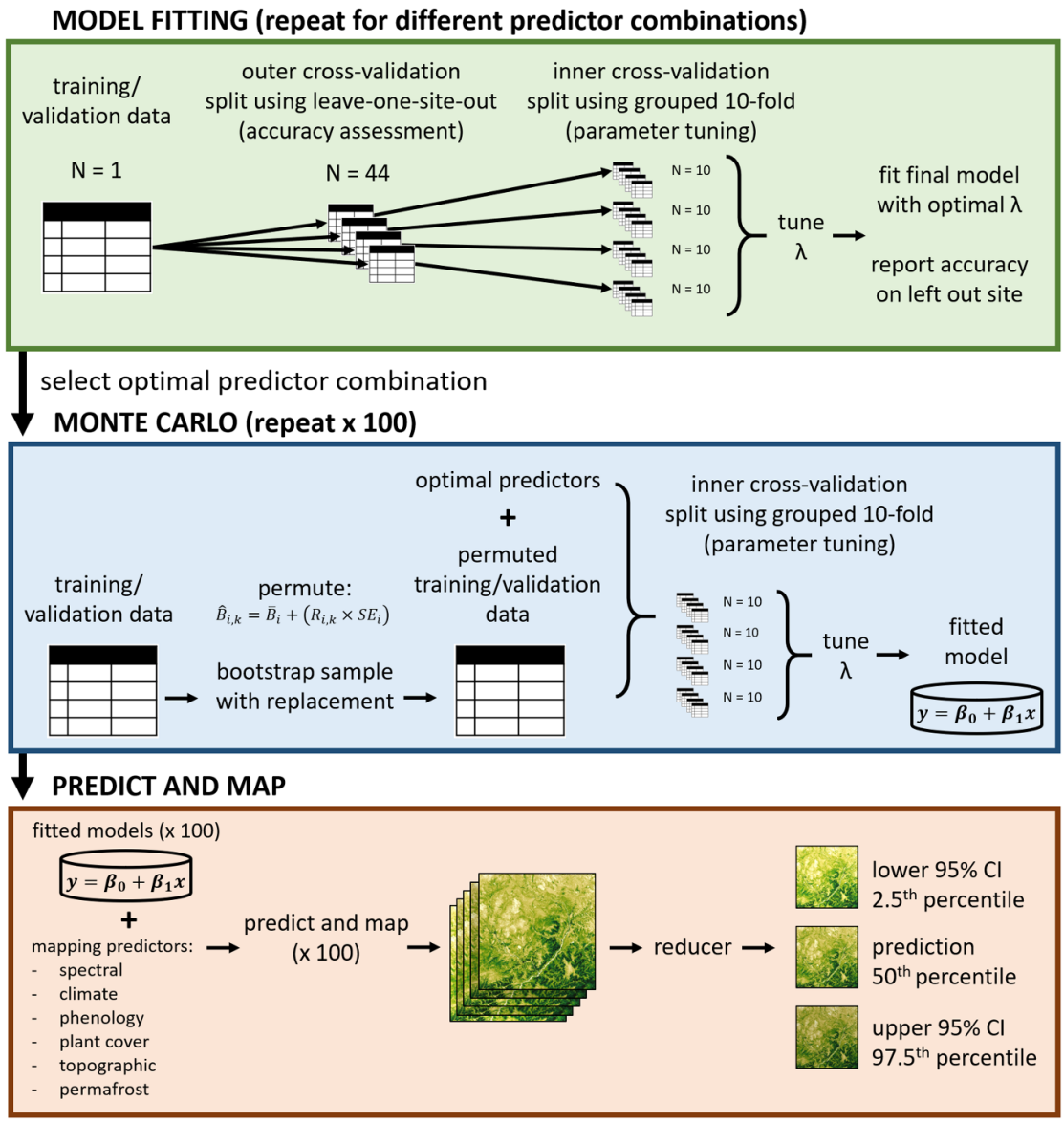

Figure 2. Flow chart showing the modeling strategy for predicting plant functional type biomass from initial model fitting (green box), to Monte Carlo uncertainty propagation (blue box), to final map products (orange box). The process shown here is repeated separately for each plant functional type.

each with a different number of predictors. More details are provided in supplementary text 2.

Using the reduced predictor sets and AGB_{PFT} as the response variable, we fit linear mixed effects models with LASSO regularization [72] using the glmmLasso package [73–75] in R v4.0.2 [76]. Site was included as a random effect, and the response variable was transformed to reduce heteroskedasticity and non-normality of the residuals. We tested both log and square root transformations and corrected predictions using Duan's smearing estimate [77]. During the model fitting process, the LASSO regularization scheme used by the glmmLasso package shrunk predictors based on their importance to the model. Some predictors were shrunk to zero and eliminated from the model.

We built a separate glmmLasso model for each PFT and used nested cross-validation to perform model selection and assess model performance. An outer leave-one-site-out cross-validation was used to assess model accuracy. An inner 10-fold cross-validation, grouped by site, was used to select the model parameter λ (supplementary text 3), which controls how heavily predictors are penalized during the LASSO regularization (figure 2, green box). The metric used to assess model accuracy within the outer cross-validation was the root-mean-squared-error (RMSE) of predictions compared to a held-out test group.

We performed this modeling process for each predictor subset and evaluated model performance as it related to number of predictors. This allowed us to

select, for each PFT, a predictor set that maximized the number of predictors while minimizing model fit and convergence issues. For each PFT, we selected the predictor subset and response variable transformation that produced the best fitting model and used these parameters to fit a final model on the full dataset. To select the final model, we used a composite metric that averaged the absolute value of normalized root-mean-squared-error (nRMSE), the absolute value of normalized mean-bias-error (nMBE) and one minus the correlation between the observed and predicted AGB_{PFT} values.

During final model fitting, we propagated uncertainty using Monte Carlo simulations ($n = 100$). We randomly permuted field-based and UAV-based estimates of AGB_{PFT} to capture uncertainty in sampling variability (field-based) and the model used to create UAV-based estimates (UAV-based). We also sampled each dataset with replacement to capture parameter uncertainty within the final model fit (figure 2, blue box) [78, 79]. We aimed to follow best practice guidelines for biomass product validation [80]. Further details about error propagation are provided in supplementary text 4.

To assess predictor importance, we standardized the coefficients (supplementary text 5) and averaged them across all 100 model fits. Predictors with higher average standardized coefficient values were deemed more important.

2.5. Mapping and validation

We created maps of AGB_{PFT} for eight years over a 35 year time series: 1985, 1990, 1995, 2000, 2005, 2010, 2015 and 2020. Using the model coefficients from each of the 100 Monte Carlo simulations, we predicted AGB_{PFT} across the study area for each time step. For each time step, the result was 100 AGB_{PFT} estimates for every pixel. We considered the best estimate to be the 50th percentile (median) and also derived a 95% confidence interval (CI) based on the 2.5th and 97.5th percentiles (figure 2, orange box).

To reduce overestimation for log transformed models the input predictors were clamped to the minimum/maximum value found in the training data −/+ 10%. Additionally, AGB_{PFT} was recorded as zero if: (a) the PFT was predicted as zero cover by Macander *et al*, 2022 [45], or (b) the land cover type was predicted as 'barren' by Wang *et al* [41].

To assess how training data source impacted modeling we compared the distribution of field-based and UAV-based data, produced final maps using both data sources, and compared them separately during validation.

We first validated our models using leave-one-site-out cross-validation. Then, final map products were compared to an existing map of shrub AGB [46] and independent harvest datasets from within [47] ($n = 11$) and outside [81, 82] ($n = 30$–38, depending on the PFT) our study area ('external validation', table S4). Based on results from model validation, we determined which training dataset (i.e. field or UAV) was best suited to predict each PFT. To make this determination, we compared actual vs predicted values and used a composite metric that averaged the absolute value of nRMSE, the absolute value of nMBE and one minus the R^2 (table 1). In cases where one training dataset was not definitively better than the other, we visually inspected the maps to make the final determination. We then produced a final regional map for each PFT using the best model.

2.6. Assessing AGB_{PFT} distribution and change over time

To explore the spatial distribution of AGB_{PFT} across the study area, we aggregated our AGB_{PFT} predictions by land cover type [41] for the year 2010. This allowed us to summarize AGB_{PFT} within commonly used categorical land cover classifications. To explore how AGB_{PFT} changed over time, we used our 35 year time series, with eight time steps, to chart trends in AGB_{PFT} across the study area. We also examined impacts of wildfires on AGB_{PFT} by tracking changes in AGB_{PFT} within burned areas. We delineated burned areas using fire polygons from the Alaska Interagency Coordination Center [83] and the Canadian National Fire Database [84] and excluded fires <200 hectares in size.

3. Results

3.1. Model/map validation, impact of training data source, and feature importance

The distribution of training data was similar between field-based and UAV-based datasets (figure S4). Both datasets exhibited right skewed distributions for all PFTs. Because of the way the data were collected and aggregated, the field-based dataset had a lower number of observations (supplementary text 1)

Based on cross-validation, external validation and visual inspection of the final map products, we found forb and lichen AGB_{PFT} were predicted slightly better by field-based models, whereas deciduous shrub, evergreen shrub and graminoid AGB_{PFT} were predicted slightly better by UAV-based models (figures S5 and S6, table 1). However, deciduous shrubs were the only PFT for which one model type (UAV-based) performed better than the other across all metrics (table 1). Final maps were produced using the best available model (figure 3).

To compare mapping results between PFTs, we normalized RMSE (nRMSE) and MBE (nMBE) using the mean of the observed data and compared nRMSE, nMBE and R^2 values amongst PFTS. Considering all accuracy metrics, we found model predictions were best for deciduous shrubs and graminoids, and worst

Table 1. Validation results for plant functional type aboveground biomass predictions. Cross-validation indicates results from the leave-one-group-out validation done as part of the modeling process. External validation indicates comparisons of predicted values to an independent dataset of field biomass harvest data. RMSE and MBE are in units of grams per meter squared. RMSE and nMBE are unitless. RMSE indicates the magnitude of the average error. nRMSE normalizes this average error based on the sample mean. MBE indicates the direction of the error i.e. underprediction (negative values) vs. overprediction (positive values). nMBE normalizes MBE based on the sample mean. R^2 indicates the proportion of variance in the dependent variable (aboveground biomass) explained by the predictors in the regression model. Composite metric was calculated by averaging the absolute value of nRMSE, the absolute value of nMBE and one minus the R^2 (table 1).

Plant functional type	RMSE (g m^{-2})	nRMSE	MBE (g m^{-2})	nMBE	R^2	Composite metric
Deciduous shrubs						
Cross-validation						
Field-based	178.4	1.2	−26.1	−0.2	0.14	0.75
UAV-based	161.3	1.0	−17.1	−0.1	0.41	0.56
External validation						
Field-based	1049.3	1.9	264.4	0.5	0.23	1.06
UAV-based	1015.0	1.8	−282.3	−0.5	0.31	1.00
Evergreen shrubs						
Cross-validation						
Field-based	56.3	0.7	−9.1	−0.1	0.10	0.57
UAV-based	63.8	0.7	−7.5	−0.1	0.07	0.58
External validation						
Field-based	109.9	1.0	−60.1	−0.5	0.11	0.80
UAV-based	100.9	0.9	−46.1	−0.4	0.15	0.72
Forbs						
Cross-validation						
Field-based	8.1	1.4	−0.7	−0.1	0.05	0.82
UAV-based	9.8	1.5	−1.2	−0.2	0.17	0.84
External validation						
Field-based	15.1	1.3	−8.4	−0.7	0.17	0.94
UAV-based	14.7	1.3	−6.8	−0.6	0.08	0.94
Graminoids						
Cross-validation						
Field-based	12.8	0.8	−1.6	−0.1	0.57	0.44
UAV-based	19.5	1.1	−2.2	−0.1	0.40	0.60
External validation						
Field-based	23.0	0.8	−9.5	−0.3	0.44	0.55
UAV-based	20.6	0.7	0.4	0.0	0.49	0.40
Lichens						
Cross-validation						
Field-based	116.1	1.3	−10.1	−0.1	0.13	0.76
UAV-based	81.9	1.6	−10.6	−0.2	0.19	0.87
External validation						
Field-based	129.1	1.5	−32.0	−0.4	0.10	0.93
UAV-based	128.0	1.5	−17.4	−0.2	0.10	0.87

for forbs and lichens (figures 4 and S7, table 1). Bias was generally negative, indicating a tendency for underprediction (table 1). Our estimates of shrub AGB were on average 109.8 [95% CI: 61.8, 147.4] g m^{-2} lower than estimates from Berner *et al* 2018 across the eastern portion of the Alaska North Slope, but we estimated higher shrub AGB in some areas with dense shrubs (figure S8).

Predictor importance varied by PFT. For deciduous shrubs, cover was the most important predictor ($\beta = 0.59$). The best evergreen shrub predictors were autumn Normalized Burn Ratio (NBR, $\beta = 21.16$) and Enhanced Vegetation Index (EVI, $\beta = 6.97$), likely because they differentiate evergreen shrubs from plants that lose their leaves in autumn. For forbs, SWIR amplitude was most important ($\beta = 7.87$), possibly because forbs (especially horsetails) are bright green early in summer but are absent or inconspicuous in spring and senesce completely in autumn. Graminoid cover was the top predictor of graminoid biomass ($\beta = 18.81$). For lichens, predictors that captured invariance in seasonal lichen color (green CC change from spring to early summer, $\beta = -26.34$) or differences in seasonal lichen visibility (NBR change from late summer to autumn, $\beta = 28.22$), were most important. This is likely because, unlike vascular plants, lichens do not change color from spring to summer, and lichen visibility increases in autumn as leaf drop reduces the amount of overtopping by shrubs. A full predictor importance comparison is provided in figure S9.

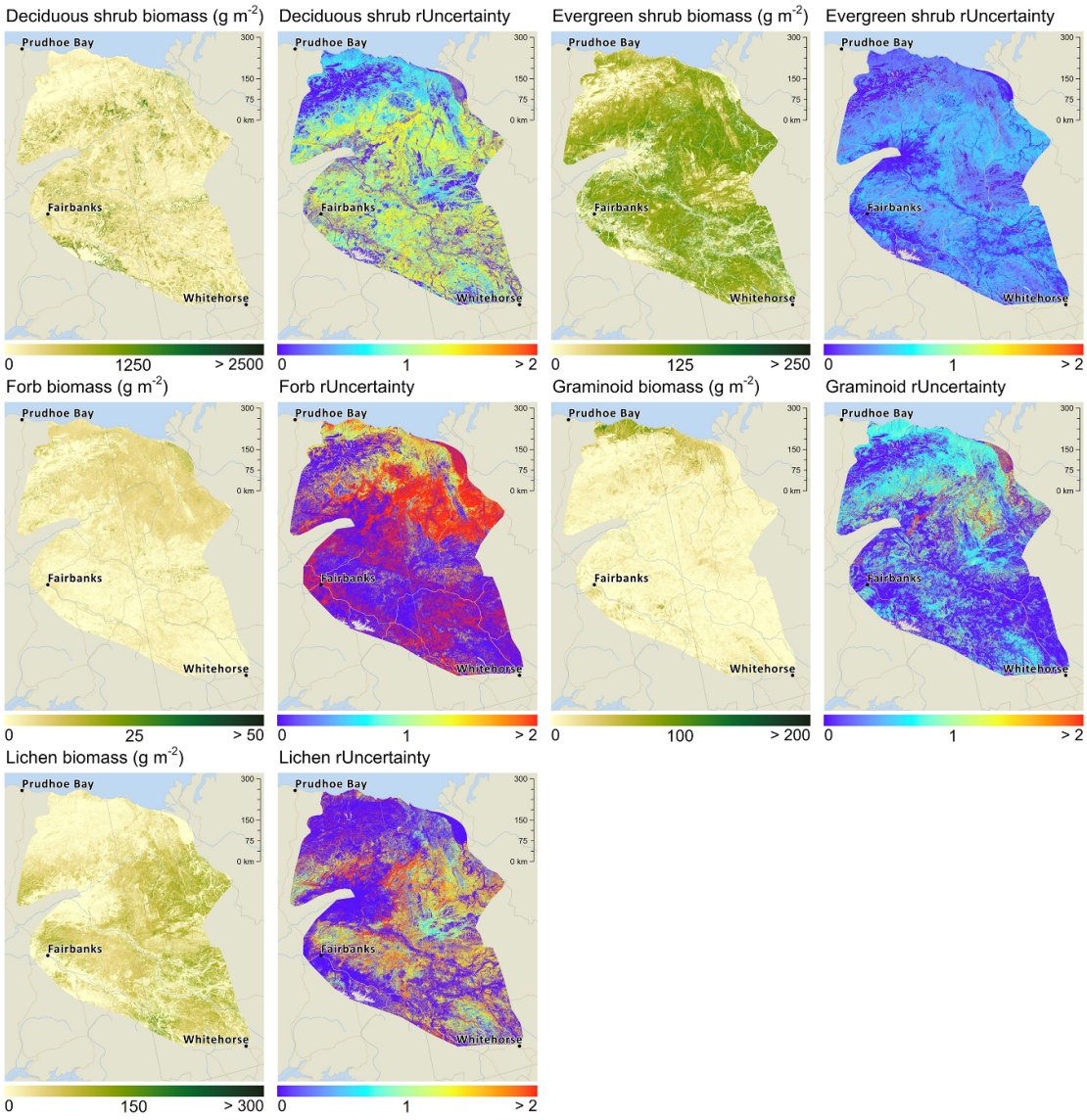

Figure 3. Final biomass maps and relative uncertainty for the year 2020. For each plant functional type, the best available model was used to create the final map. The final predictions are the median (50th percentile) of all 100 Monte Carlo iterations. Relative uncertainty is calculated as uncertainty (97.5th percentile—2.5th percentile) divided by prediction (50th percentile) and is unitless.

3.2. AGB_{PFT} distribution and change over time

We estimated plant AGB (excluding trees and mosses) totaled 178.1 [110.6, 289.0] Tg across the study area in 2020, with an average AGB density of 354.5 [214.4, 560.4] g m^{-2} (table 2). Most biomass was contained in Woodland (26%) and Tall Shrub (24%) land cover types, and biomass density was highest in Tall Shrubs (table S5). Deciduous shrubs accounted for 67% of regional non-tree/moss AGB (table 2) and constituted the majority of non-tree/moss AGB within most land cover types (figure S10). Deciduous shrub AGB density was highest in Tall Shrubs (701.3 g m^{-2}); evergreen AGB density was highest in Bogs (122.3 g m^{-2}); forb AGB density was highest in Littoral areas (7.3 g m^{-2}); graminoid AGB density was highest in Herbaceous types (27.6 g m^{-2}) and Tussock Tundra (25.2 g m^{-2}); and lichen AGB density was highest in Open Shrubs (104.0 g m^{-2}) (figure 5).

Total plant AGB (excluding trees and mosses) increased 31.1 Tg (31%) from 1985 to 2020, while AGB density increased 60.3 g m^{-2} (21%). Deciduous shrub AGB increased 32.0 Tg (37%) over the 35 year period, considerably more than any other PFT. Evergreen shrub and forb AGB increased 2.2 Tg (7%) and 0.2 Tg (15%), respectively. Conversely, lichen and graminoid AGB decreased 2.7 Tg (13%) and 0.7 Tg (15%) (table 2, figures 6 and S11).

Fires strongly influenced trends in AGB_{PFT} across the study area. Deciduous shrub, evergreen shrub and lichen AGB decreased, on average, 51%, 69% and 79% the year after fire, whereas graminoid and forb AGB increased, on average, 80% and 174% (figures 7 and S12). The largest changes in AGB_{PFT} over the study period were often located in historic fire perimeters (figure S13). Deciduous and evergreen shrub AGB increased the most in

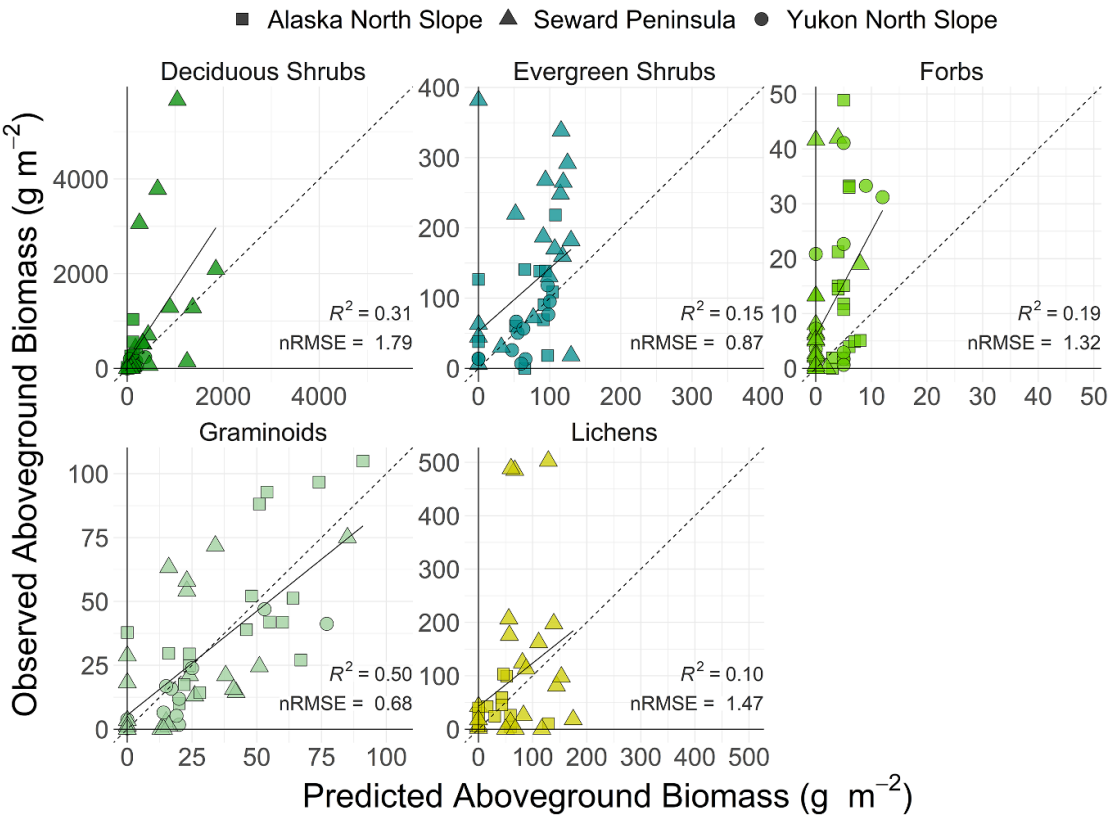

Figure 4. Independent validation results from best available models. For each plant functional type, the best model results are shown. Field-based models are used for forbs and lichens, UAV-based models are used for deciduous shrubs, evergreen shrubs and graminoids. Model predictions were compared to independent field biomass harvest data. Shapes denote the region the validation data comes from. Data from the Yukon North Slope (circles) fell within the study area. Data from the Alaska North Slope (squares) and Seward Peninsula (triangles) were outside the study area, but within similar ecosystems/vegetation community types. Biomass harvest data were compared to predictions from the biomass mapping year closest to field data collection (max difference = 2 years, mean difference = 1.1 years). Harvested area covered, at most, 0.06% of total site area and was therefore not expected to have a detectable influence on the Landsat spectral signal in the event that the harvest occurred before the mapping year. Solid lines depict best-fit regression models, while dotted lines depict 1:1 relationships.

Table 2. Total plant functional type biomass (Tg) and average plant functional type biomass density (g m^{-2}) across the study area in 1985 and 2020, as well as the change (Δ) between these periods. Brackets indicate the lower and upper 95% confidence interval (CI) from the Monte Carlo iterations.

Plant functional type	Average biomass density (g m^{-2})				Total biomass (Tg)			
	1985	2020	Δ	% Δ	1985	2020	Δ	% Δ
Deciduous shrubs	167.6	229.7	62.1	37.1	86.4	118.4	32.0	37.0
CI	[102.3, 281.9]	[138.3, 388.6]			[52.8, 145.4]	[71.3, 200.4]		
% of total					58.8%	66.5%		
Forbs	2.8	3.2	0.4	14.3	1.4	1.6	0.2	14.3
CI	[1.2, 7.6]	[1.4, 8.8]			[0.6, 3.9]	[0.7, 4.6]		
% of total					1.0%	0.9%		
Evergreen shrubs	65.6	70.0	4.4	6.7	33.8	36.0	2.2	6.5
CI	[50.9, 80.8]	[54.1, 86.2]			[26.3, 41.7]	[27.9, 45.0]		
% of total					23.0%	20.2%		
Lichens	39.5	34.4	−5.1	−12.9	20.4	17.7	−2.7	−13.2
CI	[18.4, 75.3]	[15.8, 64.3]			[9.5, 38.9]	[8.1, 33.2]		
% of total					13.9%	10.0%		
Graminoids	9.3	8.2	−1.1	−11.8	4.9	4.2	−0.7	−14.3
CI	[5.6, 13.5]	[4.9, 11.5]			[2.9, 7.0]	[2.5, 5.9]		
% of total					3.4%	2.4%		
Total	285.1	345.4	60.3	21.2	147.0	178.1	31.1	21.2
	[178.4, 214.4]	[214.4, 560.4]			[92.0, 236.8]	[110.6, 289.0]		

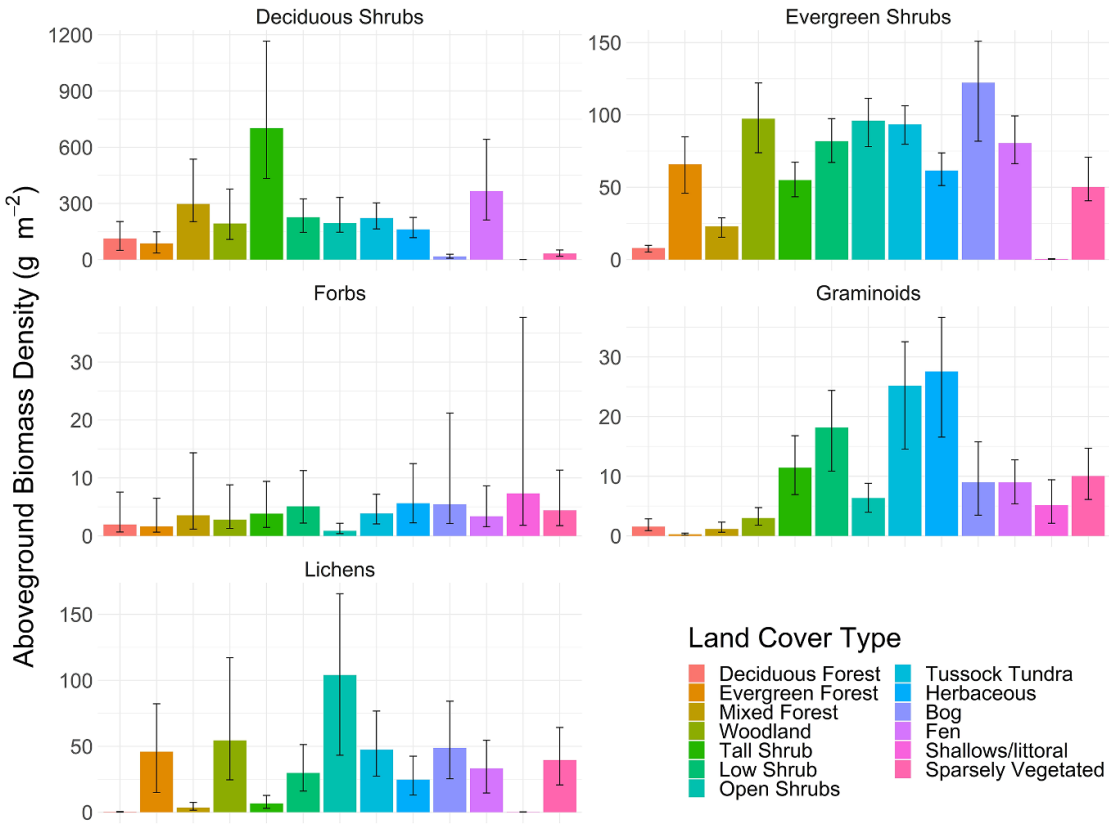

Figure 5. Average aboveground biomass density across the study area for the year 2010, broken into land cover types (colors) within plant functional types (facets). Bars show how average AGB_{PFT} density varies with land cover type. For example, lichen biomass density is highest in Open Shrubs. Error bars represent 95% confidence intervals from the Monte Carlo iterations. Note the *y*-axis ranges differ among facets.

older (21–30 year old) fire perimeters (175%, 36%), whereas forbs and graminoid AGB increased the most in newer ($\leq$10 year old) fire perimeters (246%, 63%). Lichen AGB decreased for all fire ages, by 22% on average (figure S13).

4. Discussion

4.1. Map accuracy and uncertainty

Field and UAV-based biomass data distributions were similar, lending confidence the UAV data accurately captured *in situ* conditions. Field-based data were measured directly through harvest, and thus more accurately represent on-the-ground conditions. Field data were also required to calibrate the UAV-based models. However, field data were only collected at five 0.25 m^2 quadrats per site and thus provide sparse spatial coverage relative to the spatial resolution of the Landsat sensors (900 m^2). This scale mismatch becomes more problematic as site heterogeneity increases [85]. Conversely, UAV-based data provide high spatial resolution biomass estimates across the full extent of each site, and can thus be directly aggregated to match Landsat's spatial resolution rather than extrapolated from a few small quadrats. However, UAV-based data are subject to additional sources of error, as uncertainty is introduced during the modeling process [66, 80]. We found field and UAV-based data performed similarly, with field-based models performing slightly better for forbs and lichens, and UAV-based models performing slightly better for deciduous shrubs, evergreen shrubs and graminoids (see table 1 for accuracy assessment results). UAV-based modeling added a layer of complexity, thus it is important to discern whether the added complexity improves modeling results [64, 80]. We found deciduous shrubs were the only PFT for which UAV-based modeling produced consistently better results (see table 1 for accuracy assessment results). Deciduous shrubs were likely modeled best by UAV-based data because they often occur in the canopy and have more vertical structure than other PFTs besides trees. UAV AGB_{PFT} predictions were produced using Structure from Motion technology, which cannot penetrate vegetation canopies [66]. UAV-based biomass estimation of shrubs might therefore be improved with canopy-penetrating lidar technology that can produce more reliable mapping of the ground surface [64].

Independent evaluation of biomass maps is difficult due to a lack of biomass harvest datasets partitioned by PFT. To independently validate our results, we therefore relied on some data collected outside our study area [81, 82]. We found graminoids

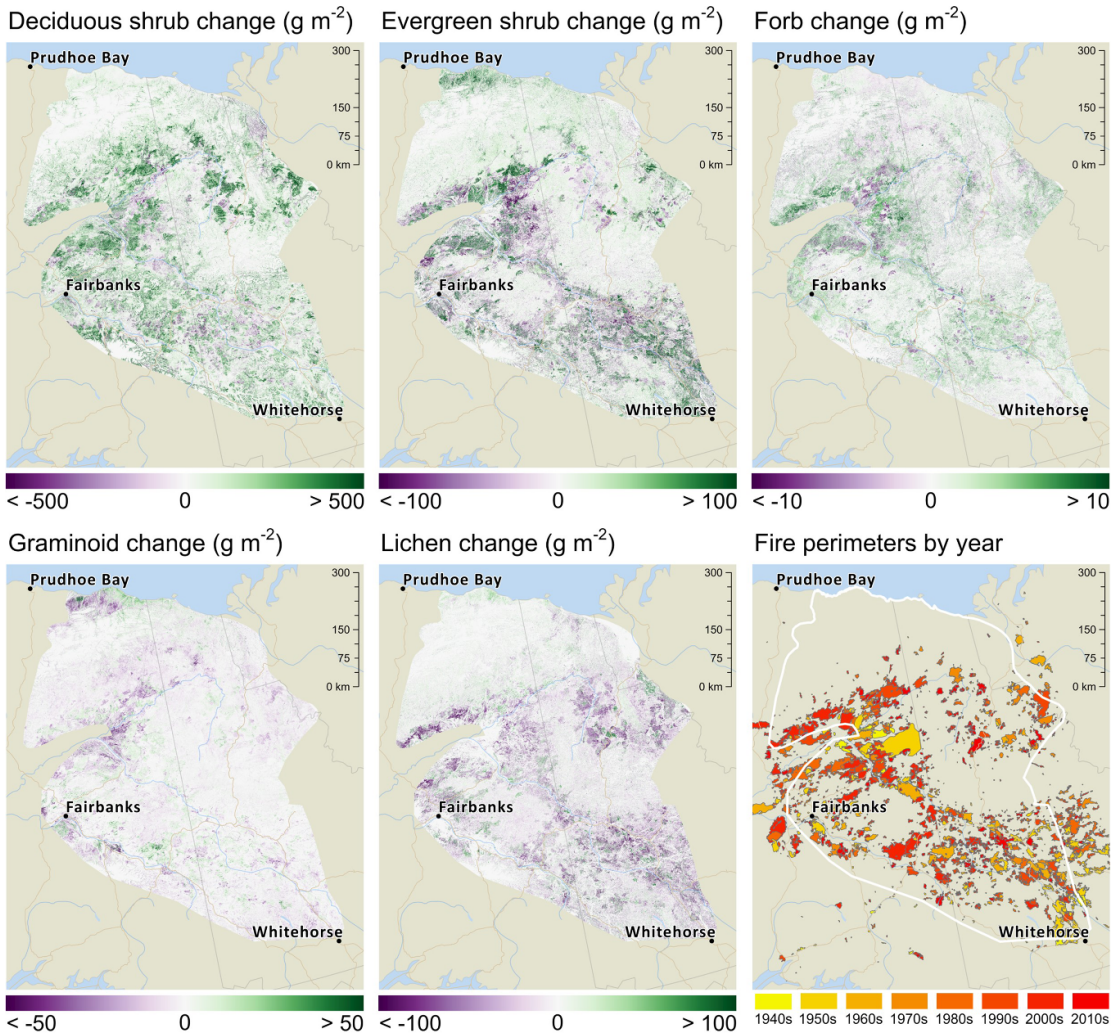

Figure 6. Change in plant functional type aboveground biomass between 1985 and 2020 across the study area. The bottom right panel shows historic fire perimeters, colored by decade. The white outline shows the study area.

were predicted best, comparing well during cross-validation and external validation. Deciduous shrubs performed well during cross-validation, but less well during external validation. This is likely because our data set had limited observations where shrub AGB was high. For example, we had only one observation with deciduous shrub AGB > 4000 g m^{-2}. Our model therefore tended to underpredict deciduous shrub biomass as compared to external validation data.

Our AGB_{PFT} estimates were likely less accurate in more heavily forested areas because (a) our training/validation site locations were concentrated in non-forested areas and (b) tree canopy obscures understory vegetation in satellite imagery. However, we took steps to facilitate prediction of understory AGB_{PFT} in areas with trees. First, tree cover was included as a predictor in the AGB_{PFT} models. This enabled prediction of understory AGB by allowing the model to differentiate AGB_{PFT} spectral signals in areas with and without trees. Second, we used PFT cover maps [45] to mask our AGB_{PFT} maps. Pixels with zero percent cover for a particular PFT were assigned zero AGB for that PFT. This masked out AGB_{PFT} in some areas with dense tree cover. We acknowledge that despite these efforts, AGB_{PFT} predictions in forested areas are subject to error. Notably, tree biomass might be erroneously associated with shrubs and/or AGB_{PFT} might be underestimated where it is obscured by tree canopy.

Estimating uncertainty in map products is crucial to understanding their accuracy across time and space, and to facilitate comparison with other map products. We used a Monte Carlo approach to propagate major sources of uncertainty through our modeling process. Ideally, uncertainty estimation would incorporate error in the reference data including the modeling process used to produce UAV-based AGB_{PFT} estimates, while also incorporating error in the predictor variables, sampling variability, and uncertainty in the final model building process [80]. We did not include error/uncertainty in the remotely sensed predictor data due to computational limitations. We also likely underestimated uncertainty in

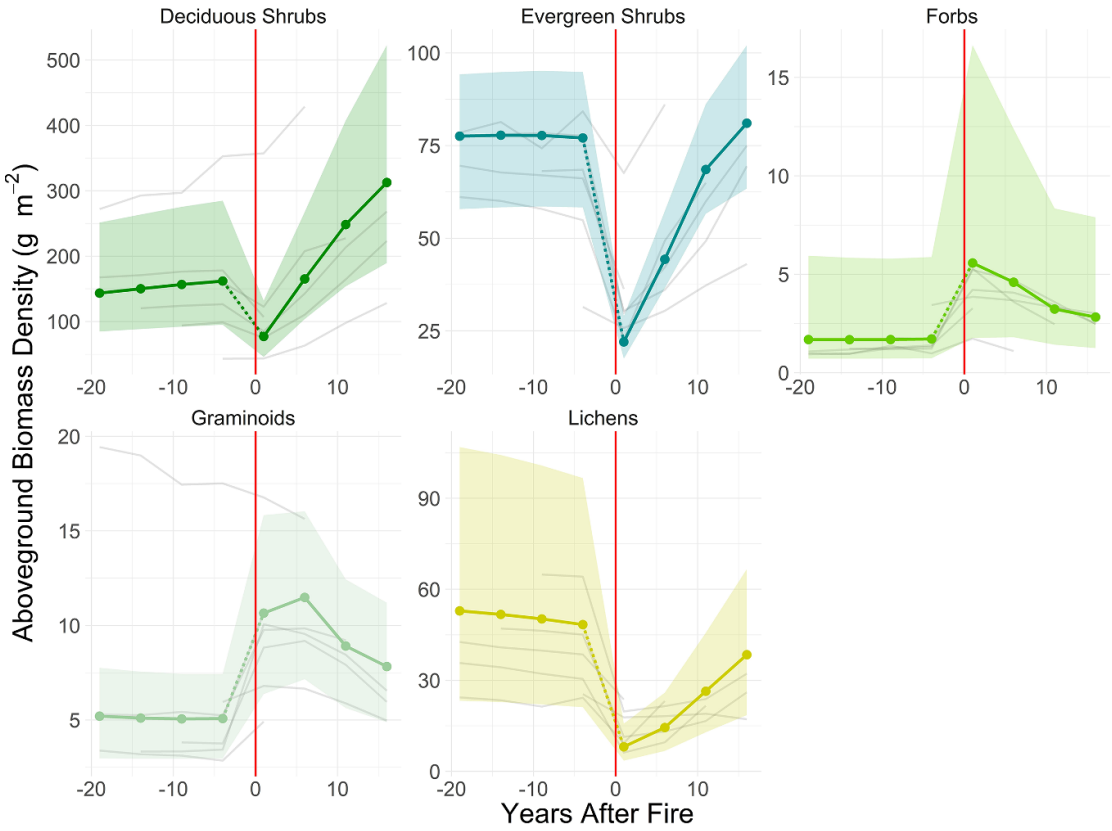

Figure 7. Change in average AGB_{PFT} density through time within the perimeters of fires that occurred in 2004. The 2004 fire season burned the most acres of any season on record for Alaska. The biomass mapping year 2005 illustrates conditions one year after the 2004 fires and thus captures immediate post-fire conditions. Trends in AGB_{PFT} density within fire perimeters are represented by colored points and lines. Dashed lines indicate the trend from pre-fire to post-fire. The year of the fire is indicated by a vertical red line. Years after fire are shown on the *x*-axis, with negative numbers indicating years before fire. Ribbons represent 95% confidence intervals from the Monte Carlo iterations. Trends from other fire years are shown in grey. These trends are mapped for fire years 1989, 1994, 1999, 2009, 2014 and 2019 (i.e. fires that occurred exactly one year before a year for which biomass is mapped).

UAV modeling, which involved several stages that each added uncertainty [66]. Uncertainty in scaling from field data to UAV imagery is likely to be an important source of error, therefore the use of UAV data as an intermediate modeling step should be carefully considered in the context of mapping objectives. It remains challenging to account for the myriad sources of uncertainty that arise when modeling regional biomass, especially when incorporating field, UAV, satellite, and environmental datasets.

4.2. Land cover analysis

Deciduous shrubs made up the majority (67%) of total plant AGB (excluding trees and mosses) across the study area in 2020. On the Alaska North Slope, previous research estimated shrubs accounted for 43% of total AGB from 2007 to 2016 [46]. Our estimate is likely higher because shrub dominance tends to be higher in areas with warmer summers [46, 86]. For example, across the Alaska North Slope, Berner *et al* 2018 found shrub dominance increased from about 30% to 50% between areas with the lowest June temperatures (1.4 °C) and the warmest June temperatures (11.3 °C). Conversely, graminoids made up only a small percentage (2%) of total AGB across the study area, despite being the second most common PFT by cover [45]. Deciduous shrub AGB constituted the majority of total AGB for most land cover types—even types named for dominance of a different PFT (e.g. graminoids in Tussock Tundra). This highlights not only the important role of deciduous shrubs in regional plant communities, but also the importance of quantifying PFT biomass in addition to cover [87].

4.3. AGB_{PFT} change over time

Our analysis showed a 31% increase in total AGB (excluding trees and mosses) from 1985 to 2020. This is surprisingly consistent with an estimated 32% increase in total AGB from 1982 to 2010 across Northern Alaska derived from AVHRR NDVI [88], despite vastly different spatial resolutions (30 m vs 12.5 km). Furthermore, we found increasing AGB was primarily driven by deciduous shrubs (37%). Similarly, there have been large increases in deciduous shrub cover in recent decades across Alaska and the Yukon Territory [45]. These increases are consistent with trends of warming-induced deciduous shrub expansion across much of the Low Arctic [4, 5, 89].

Our study documents large regional increases in tundra AGB linked primarily to deciduous shrubs, while also revealing more subtle shifts in the AGB of other PFTs. We found evergreen shrub and forb AGB increased to a lesser extent than deciduous shrubs (7%, 14%), whereas graminoid and lichen AGB decreased (14%, 13%). Meta-analyses of warming experiments across the Arctic report a standardized mean difference (unitless) of +11 for deciduous shrubs, +24 for low shrubs, +36 for tall shrubs, +5 for evergreen shrubs, +5 for graminoids, +1 for forbs and −17 for lichens [4]. The direction and magnitude of changes reported by this meta-analysis were consistent with our results, with the exception of graminoids, for which we reported a decrease. Graminoid decreases we documented could be due to overtopping from expanding shrubs which could both obscure graminoid cover in satellite imagery and cause on-the-ground declines via light competition [45, 53].

Heterogeneity is inherent in patterns of Arctic greening and vegetation change. For example, greening can be caused by shifts in relative abundance of different PFTs, or by more uniform increases in growth of existing vegetation [2, 10, 15]. The shrub AGB increases we report likely capture both of these greening pathways. Within PFTs, species are likely to respond differently to warming [5, 44, 90]. Our maps aggregate vegetation at the PFT level, but advances in spectral and spatial resolution of remotely sensed imagery might facilitate mapping of species level vegetation change [44, 91]. Disturbances such as wildfire can cause abrupt and patchy vegetation change. Finally, landscape and environmental conditions, particularly soil moisture, influence where vegetation shifts occur [2, 10, 15]. We found the largest increases in deciduous shrub AGB typically occurred in wetter areas along riverbanks and in drainages, as well as within 11–30 year old fire perimeters, which is consistent with prior research in northern Alaska and Canada [10, 92, 93]. Evergreen shrub AGB similarly increased in intermediate age fire perimeters, and on the Alaska North Slope, which aligns with strong trends of greening recorded for the Alaska coastal plain [94]. Decreases in graminoid, forb and lichen AGB often occurred in areas with increasing shrub AGB, suggesting these declines might be driven by competition [53]. Graminoid and lichen AGB decrease were both widespread across the study area. However, lichen declines were often located within fire perimeters, whereas graminoid declines were less closely tied to fire and were prevalent along the Alaska North Slope. Changes in graminoid and forb AGB were pronounced in the Yukon Flats, although this should be interpreted with caution as we did not have training or validation data in this area.

4.4. Fire impacts on AGB_{PFT}

Fire had a significant impact on AGB_{PFT} distribution and trends. In general, deciduous shrub, evergreen shrub and lichen biomass decreased the year following fire whereas graminoid and forb biomass increased. Deciduous shrubs recovered relatively quickly after fire, generally returning to pre-fire AGB levels 5 years after fire and exceeding pre-fire conditions as succession continued, in line with overall trends of increasing shrub AGB. These trends were consistent with tundra fire research done in Alaska that suggests vegetation recovers to pre-fire levels approximately 3 years after fire [95, 96]. However, other research suggests recovery periods for deciduous shrubs are generally longer (>10 years) [97, 98]. A longer time-frame for shrub recovery is suggested by figure S13, where deciduous and evergreen shrub AGB increase was greatest for intermediate age fires. Within 11–30 year old fire perimeters, shrub AGB increase regularly exceeded 100%, demonstrating the ability of fires to facilitate deciduous shrub and tree growth [95, 96, 99–102]. Boreal forest fires burn more severely and take longer to recover. However, they too seem to promote growth of shrubs and are often characterized by an intermediate stage of deciduous shrub growth and dominance [99–102].

Lichens experienced the largest relative declines in AGB post-fire. Lichen AGB decrease within fire perimeters regularly exceeded 25%, which was nearly double that experienced across the full study area. Lichens were also slowest to recover, in several instances not reaching pre-fire levels, even 30 years after fire. This is consistent with research documenting susceptibility of lichens to combustion, and slow recovery of lichens after fire [50, 103, 104]. Fire induced declines in lichen have serious implications for wildlife as lichen are an important food source for caribou. Caribou have been known to avoid burned areas up to 50 years post-fire [50, 105].

We found graminoid and forb AGB increased after fire, then declined to pre-fire levels as succession continued. Sedges and grasses are able to re-sprout from surviving roots and rhizomes, and thus recover quickly following fire [95, 97, 98, 106]. Graminoids then show increased productivity as they are released from competition with more slowly regenerating shrubs [106]. These factors might explain why graminoid AGB increased the year after fire. Forbs also respond positively to fire [102, 107, 108], and horsetails are known to survive fire due to deep rhizoids [109].

Within fire perimeters, forb and graminoid AGB increased in newer fire perimeters, but not those of intermediate age, likely because these PFTs are some of the first colonizers of post-fire landscapes [102, 107, 108]. Areas of forb and graminoid decrease within intermediate age fires were often correlated

with areas of shrub increase, suggesting these PFTs were outcompeted as shrub growth accelerated.

5. Conclusion

The maps we present move beyond two-dimensions and capture the composition and structure of vegetation across Alaska and northwest Canada over the past four decades. Mapping biomass by PFT makes it possible to characterize spatial and temporal patterns of vegetation change in the Arctic. We report increases in deciduous and evergreen shrub biomass that are consistent with greening trends taking place across much of the Arctic. Conversely, we observed decreases in lichens and graminoid biomass, which were often coincident with shrub increase. Fires were influential in driving spatial and temporal patterns of AGB. Our maps capture patterns of post-fire succession consistent with previous research, notably early succession driven by an increase in graminoids and forbs, initial decreases in deciduous and evergreen shrubs, and long-lasting decreases in lichens. We present an example of a multi-scale modeling approach that could be applied to other regions, with appropriate training/validation data inputs. Mapping vegetation biomass remains challenging, due in large part to the difficulty of acquiring biomass harvest data. As biomass datasets continue to grow, a centralized database of harmonized AGB would facilitate future mapping efforts. Advancements in lidar technology (satellite, airborne and UAV-based) are also likely to further biomass mapping efforts as lidar is able to penetrate vegetation canopies and better reconstruct ground surfaces and canopy heights.

Data availability statement

The data that support the findings of this study are available upon reasonable request from the authors. DOI: 10.18739/A2Q52FF2B.

Acknowledgments

This research was supported by the National Science Foundation Graduate Research Fellowship under Grant No. 1938054 (to KMO) and NASA ABoVE Grants NNX17AE44G and 80NSSC19M0112 (to SJG). Additional support was provided by NASA New Investigator Program Grant 80NSSC21K1364 (to LTB). The authors extend thanks to all those who assisted in collecting the high-quality field data that made this research possible: Craig Townsend, Joël Potié, Elis Juhlin, Abby Rutrough, Aerin Jacob, Kayla Arey, Laurence Carter, Martin Kienzler, Sonny Parker, Hayleigh Conway and Andrew Davies. Data analysis was facilitated by NAU's Monsoon computing cluster, funded by Arizona's Technology and Research Initiative Fund. The authors thank the Monsoon team for technical assistance during data analysis. Analyses were improved by feedback from GEODE lab members at Northern Arizona University (NAU), and the manuscript was much improved by feedback from three anonymous reviewers.

Conflict of interest

The authors declare there are no competing interest.

ORCID iDs

Kathleen M Orndahl https://orcid.org/0000-0002-4873-4375
Matthew J Macander https://orcid.org/0000-0003-2808-208X
Logan T Berner https://orcid.org/0000-0001-8947-0479
Scott J Goetz https://orcid.org/0000-0002-6326-4308

References

[1] Rantanen M, Karpechko A Y, Lipponen A, Nordling K, Hyvärinen O, Ruosteenoja K, Vihma T and Laaksonen A 2022 The Arctic has warmed nearly four times faster than the globe since 1979 *Commun. Earth Environ.* **3** 1–10
[2] Bjorkman A D *et al* 2018 Plant functional trait change across a warming tundra biome *Nature* **562** 57–62
[3] Mekonnen Z A *et al* 2021 Arctic tundra shrubification: a review of mechanisms and impacts on ecosystem carbon balance *Environ. Res. Lett.* **16** 053001
[4] Elmendorf S C *et al* 2012 Global assessment of experimental climate warming on tundra vegetation: heterogeneity over space and time *Ecol. Lett.* **15** 164–75
[5] Elmendorf S C *et al* 2012 Plot-scale evidence of tundra vegetation change and links to recent summer warming *Nat. Clim. Change* **2** 453–7
[6] Myers-Smith I H *et al* 2019 Eighteen years of ecological monitoring reveals multiple lines of evidence for tundra vegetation change *Ecol. Monogr.* **89** e01351
[7] Wookey P A *et al* 2009 Ecosystem feedbacks and cascade processes: understanding their role in the responses of Arctic and alpine ecosystems to environmental change *Glob. Change Biol.* **15** 1153–72
[8] Berner L T *et al* 2020 Summer warming explains widespread but not uniform greening in the Arctic tundra biome *Nat. Commun.* **11** 1–12
[9] Raynolds M K, Walker D A, Epstein H E, Pinzon J E and Tucker C J 2012 A new estimate of tundra-biome phytomass from trans-Arctic field data and AVHRR NDVI *Remote Sens.Lett.* **3** 403–11
[10] Campbell T K F, Lantz T C, Fraser R H and Hogan D 2021 High Arctic vegetation change mediated by hydrological conditions *Ecosystems* **24** 106–21
[11] Frost G V *et al* 2021 Tundra Greenness (available at: https://repository.library.noaa.gov/view/noaa/34310)
[12] Treharne R, Bjerke J W, Tømmervik H, Stendardi L and Phoenix G K 2019 Arctic browning: impacts of extreme climatic events on heathland ecosystem CO_2 fluxes *Glob. Change Biol.* **25** 489–503
[13] Phoenix G K and Bjerke J W 2016 Arctic browning: extreme events and trends reversing arctic greening *Glob. Change Biol.* **22** 2960–2
[14] Epstein H *et al* 2018 Tundra greenness *NOAA Arctic Report Card* (available at: www.arctic.noaa.gov/reportcard/)

[15] Myers-Smith I H et al 2020 Complexity revealed in the greening of the Arctic Nat. Clim. Change 10 106–17
[16] Rees W G, Hofgaard A, Boudreau S, Cairns D M, Harper K, Mamet S, Mathisen I, Swirad Z and Tutubalina O 2020 Is subarctic forest advance able to keep pace with climate change? Glob. Change Biol. 26 3965–77
[17] Beck P S A, Juday G P, Alix C, Barber V A, Winslow S E, Sousa E E, Heiser P, Herriges J D and Goetz S J 2011 Changes in forest productivity across Alaska consistent with biome shift Ecol. Lett. 14 373–9
[18] Frost G V and Epstein H E 2014 Tall shrub and tree expansion in Siberian tundra ecotones since the 1960s Glob. Change Biol. 20 1264–77
[19] Baltzer J L et al 2021 Increasing fire and the decline of fire adapted black spruce in the boreal forest Proc. Natl Acad. Sci. USA 118 e2024872118
[20] Peng C, Ma Z, Lei X, Zhu Q, Chen H, Wang W, Liu S, Li W, Fang X and Zhou X 2011 A drought-induced pervasive increase in tree mortality across Canada's boreal forests Nat. Clim. Change 1 467–71
[21] Berner L T and Goetz S J 2022 Satellite observations document trends consistent with a boreal forest biome shift Glob. Change Biol. 28 3275–92
[22] Dial R J, Maher C T, Hewitt R E and Sullivan P F 2022 Sufficient conditions for rapid range expansion of a boreal conifer Nature 608 546–51
[23] Loranty M M and Goetz S J 2012 Shrub expansion and climate feedbacks in Arctic tundra Environ. Res. Lett. 7 011005
[24] Loranty M M, Goetz S J and Beck P S A 2011 Tundra vegetation effects on pan-Arctic albedo Environ. Res. Lett. 6 024014
[25] Sturm M 2005 Changing snow and shrub conditions affect albedo with global implications J. Geophys. Res. 110 1–13
[26] Mack M C, Schuur E A G, Bret-Harte M S, Shaver G R and Chapin F S 2004 Ecosystem carbon storage in arctic tundra reduce by long-term nutrient fertilization Nature 431 440–3
[27] Abbott B W et al 2016 Biomass offsets little or none of permafrost carbon release from soils, streams, and wildfire: an expert assessment Environ. Res. Lett. 11 034014
[28] Lafleur P M and Humphreys E R 2018 Tundra shrub effects on growing season energy and carbon dioxide exchange Environ. Res. Lett. 13 055001
[29] Hobbie S E and Chapin F S 1998 The response of Tundra plant biomass, aboveground production, nitrogen, and CO_2 flux to experimental warming Ecology 79 1526–44
[30] Higuera P E, Brubaker L B, Anderson P M, Brown T A, Kennedy A T and Hu F S 2008 Frequent fires in ancient shrub Tundra: implications of paleorecords for Arctic environmental change PLoS One 3 1–7
[31] Post E et al 2009 Ecological dynamics across the arctic associated with recent climate change Science 325 1355–8
[32] Tape K D, Gustine D D, Ruess R W, Adams L G and Clark J A 2016 Range expansion of moose in Arctic Alaska linked to warming and increased shrub habitat PLoS One 11 e0152636
[33] Schuur E A G et al 2015 Climate change and the permafrost carbon feedback Nature 520 171–9
[34] Lawrence D M and Swenson S C 2011 Permafrost response to increasing Arctic shrub abundance depends on the relative influence of shrubs on local soil cooling versus large-scale climate warming Environ. Res. Lett. 6 045504
[35] Nauta A L et al 2015 Permafrost collapse after shrub removal shifts tundra ecosystem to a methane source Nat. Clim. Change 5 67–70
[36] Loranty M M et al 2018 Reviews and syntheses: changing ecosystem influences on soil thermal regimes in northern high-latitude permafrost regions Biogeosciences 15 5287–313
[37] Ju J and Masek J G 2016 The vegetation greenness trend in Canada and US Alaska from 1984–2012 Landsat data Remote Sens. Environ. 176 1–16
[38] Guay K C, Beck P S A, Berner L T, Goetz S J, Baccini A and Buermann W 2014 Vegetation productivity patterns at high northern latitudes: a multi-sensor satellite data assessment Glob. Change Biol. 20 3147–58
[39] Beck P S A and Goetz S J 2011 Satellite observations of high northern latitude vegetation productivity changes between 1982 and 2008: ecological variability and regional differences Environ. Res. Lett. 6 045501
[40] Wullschleger S D, Epstein H E, Box E O, Euskirchen E S, Goswami S, Iversen C M, Kattge J, Norby R J, Van Bodegom P M and Xu X 2014 Plant functional types in Earth system models: past experiences and future directions for application of dynamic vegetation models in high-latitude ecosystems Ann. Bot. 114 1–16
[41] Wang J A, Sulla-Menashe D, Woodcock C E, Sonnentag O, Keeling R F and Friedl M A 2019 ABoVE: Landsat-derived Annual Dominant Land Cover across above Core Domain, 1984–2014 (Oak Ridge, TN: ORNL DAAC)
[42] Macander M J, Frost G V, Nelson P R and Swingley C S 2017 Regional quantitative cover mapping of tundra plant functional types in Arctic Alaska Remote Sens. 9 1–26
[43] Macander M J et al 2020 Lichen cover mapping for caribou ranges in interior Alaska and Yukon Environ. Res. Lett. 15 055001
[44] Nawrocki T W, Carlson M L, Osnas J L D, Trammell E J and Witmer F D W 2020 Regional mapping of species-level continuous foliar cover: beyond categorical vegetation mapping Ecol. Appl. 30 e02081
[45] Macander M J, Nelson P R, Nawrocki T W, Frost G V, Orndahl K M, Palm E C, Wells A F and Goetz S J 2022 Time-series maps reveal widespread change in plant functional type cover across arctic and boreal Alaska and Yukon Environ. Res. Lett. 17 054042
[46] Berner L T, Jantz P, Tape K D and Goetz S J 2018 Tundra plant above-ground biomass and shrub dominance mapped across the North Slope of Alaska Environ. Res. Lett. 13 035002
[47] Chen W, Chen W, Li J, Zhang Y, Fraser R, Olthof I, Leblanc S G and Chen Z 2012 Mapping aboveground and foliage biomass over the Porcupine Caribou habitat in Northern Yukon and Alaska using Landsat and JERS-1/SAR data Remote Sensing of Biomass – Principles and Applications ed T Fatoyinb (Rijeka: IntechOpen) pp 231–52
[48] Hudson J M G and Henry G H R 2009 Increased plant biomass in a high Arctic heath community from 1981 to 2008 Ecology 90 2657–63
[49] Vowles T and Björk R G 2019 Implications of evergreen shrub expansion in the Arctic J. Ecol. 107 650–5
[50] Joly K, Jandt R R and Klein D R 2009 Decrease of lichens in Arctic ecosystems: the role of wildfire, caribou, reindeer, competition and climate in north-western Alaska Polar Res. 28 433–42
[51] Chapin F S, Shaver G R, Giblin A E, Nadelhoffer K J and Laundre J A 1995 Responses of Arctic tundra to experimental and observed changes in climate Ecology 76 694–711
[52] Walker M D et al 2006 Plant community responses to experimental warming across the tundra biome Proc. Natl Acad. Sci. 103 1342–6
[53] Mekonnen Z A, Riley W J and Grant R F 2018 Accelerated nutrient cycling and increased light competition will lead to 21st century shrub expansion in North American Arctic tundra J. Geophys. Res. 123 1683–701
[54] Vors L S and Boyce M S 2009 Global declines of caribou and reindeer Glob. Change Biol. 15 2626–33
[55] Olofsson J and Post E 2018 Effects of large herbivores on tundra vegetation in a changing climate, and implications for rewilding Phil. Trans. R. Soc. B 373 20170437
[56] Lantz T C, Gergel S E and Henry G H R 2010 Response of green alder (*Alnus viridis* subsp. *fruticosa*) patch dynamics and plant community composition to fire and regional temperature in north-western Canada J. Biogeogr. 37 1597–610

[57] Tape K, Sturm M and Racine C 2006 The evidence for shrub expansion in Northern Alaska and the Pan-Arctic *Glob. Change Biol.* **12** 686–702
[58] Greaves H E, Vierling L A, Eitel J U H, Boelman N T, Magney T S, Prager C M and Griffin K L 2015 Estimating aboveground biomass and leaf area of low-stature Arctic shrubs with terrestrial LiDAR *Remote Sens. Environ.* **164** 26–35
[59] Greaves H E, Vierling L A, Eitel J U H, Boelman N T, Magney T S, Prager C M and Griffin K L 2016 High-resolution mapping of aboveground shrub biomass in Arctic tundra using airborne lidar and imagery *Remote Sens. Environ.* **184** 361–73
[60] Alonzo M, Dial R J, Schulz B K, Andersen H-E, Lewis-Clark E, Cook B D and Morton D C 2020 Mapping tall shrub biomass in Alaska at landscape scale using structure-from-motion photogrammetry and lidar *Remote Sens. Environ.* **245** 111841
[61] Fraser R H, Olthof I, Lantz T C and Schmitt C 2016 UAV photogrammetry for mapping vegetation in the low-Arctic *Arct. Sci.* **2** 79–102
[62] Cunliffe A M, J Assmann J N, Daskalova G, Kerby J T and Myers-Smith I H 2020 Aboveground biomass corresponds strongly with drone-derived canopy height but weakly with greenness (NDVI) in a shrub tundra landscape *Environ. Res. Lett.* **15** 125004
[63] Matasci G, Hermosilla T, Wulder M A, White J C, Coops N C, Hobart G W and Zald H S J 2018 Large-area mapping of Canadian boreal forest cover, height, biomass and other structural attributes using Landsat composites and lidar plots *Remote Sens. Environ.* **209** 90–106
[64] Poley L G and McDermid G J 2020 A systematic review of the factors influencing the estimation of vegetation aboveground biomass using unmanned aerial systems *Remote Sens.* **12** 1052
[65] Riihimäki H, Luoto M and Heiskanen J 2019 Estimating fractional cover of tundra vegetation at multiple scales using unmanned aerial systems and optical satellite data *Remote Sens. Environ.* **224** 119–32
[66] Orndahl K M, Ehlers L P W, Herriges J D, Pernick R E, Hebblewhite M and Goetz S J 2022 Mapping tundra ecosystem plant functional type cover, height and aboveground biomass in Alaska and northwest Canada using unmanned aerial vehicles *Arct. Sci.* 1–16
[67] Gorelick N, Hancher M, Dixon M, Ilyushchenko S, Thau D and Moore R 2017 Google Earth engine: planetary-scale geospatial analysis for everyone *Remote Sens. Environ.* **202** 18–27
[68] Zhu Z, Wang S and Woodcock C E 2015 Improvement and expansion of the Fmask algorithm: cloud, cloud shadow, and snow detection for Landsats 4–7, 8, and Sentinel 2 images *Remote Sens. Environ.* **159** 269–77
[69] Roy D P, Kovalskyy V, Zhang H K, Vermote E F, Yan L, Kumar S S and Egorov A 2016 Characterization of Landsat-7 to Landsat-8 reflective wavelength and normalized difference vegetation index continuity *Remote Sens. Environ.* **185** 57–70
[70] Zhu Z and Woodcock C E 2014 Continuous change detection and classification of land cover using all available Landsat data *Remote Sens. Environ.* **144** 152–71
[71] Wang J A, Sulla-Menashe D, Woodcock C E, Sonnentag O, Keeling R F and Friedl M A 2020 Extensive land cover change across Arctic–Boreal Northwestern North America from disturbance and climate forcing *Glob. Change Biol.* **26** 807–22
[72] Tibshirani R 1996 Regression shrinkage and selection via the lasso *J. R. Stat. Soc.* B **58** 267–88
[73] Groll A 2017 "glmmLasso": variable selection for generalized linear mixed models by L1-Penalized Estimation (available at: https://mirror.rcg.sfu.ca/mirror/CRAN/web/packages/glmmLasso/glmmLasso.pdf)
[74] Groll A and Tutz G 2014 Variable selection for generalized linear mixed models by L1-penalized estimation *Stat. Comput.* **24** 137–54
[75] Schelldorfer J, Meier L and Bühlmann P 2014 GLMMLasso: an algorithm for high-dimensional generalized linear mixed models using $\ell 1$-penalization *J. Comput. Graph. Stat.* **23** 460–77
[76] R Core Team 2020 R: a language and environment for statistical computing (Vienna: R Foundation for Statistical Computing) (available at: www.r-project.org/)
[77] Duan N 1983 Smearing estimate: a nonparametric retransformation method *J. Am. Stat. Assoc.* **78** 605–10
[78] Efron B and Tibshirani R 1993 *An Introduction to the Bootstrap* (New York: Chapman & Hall)
[79] Davidson A C and Hinkley D V 1997 *Bootstrap Methods and Their Application* 1st edn (Cambridge: Cambridge University Press)
[80] Duncanson L, Disney M, Armston J, Nickeson J, Minor D and Camacho F 2021 Aboveground woody biomass product validation good practices protocol 1.0 (Committee on Earth Observation Satellites)
[81] Raynolds M K 2018 *Arctic Vegetation Plots ATLAS Project North Slope and Seward Peninsula, AK, 1998–2000* (Oak Ridge, TN: ORNL DAAC)
[82] Salmon V, Iversen C M, Breen A L, VanderStel H and Childs J 2019 NGEE Arctic plant traits: plant aboveground biomass, NPP and traits, Kougarok Road mile marker 64, Seward Peninsula, Alaska, beginning 2016 *(NGEE Arctic, Oak Ridge National Laboratory, US Department of Energy)* (https://doi.org/10.5440/1346199)
[83] Alaska Interagency Coordination Center 2021 Alaska Fire History Polygons 1940–2021 (available at: https://fire.ak.blm.gov/predsvcs/maps.php)
[84] Natural Resources Canada 2020 Canadian National Fire Database (available at: https://cwfis.cfs.nrcan.gc.ca/ha/nfdb)
[85] Siewert M B and Olofsson J 2020 Scale-dependency of Arctic ecosystem properties revealed by UAV *Environ. Res. Lett.* **15** 129601
[86] Epstein H E, Walker D A, Raynolds M K, Jia G J, Kelley A M, Epstein C :, Walker D A, Raynolds M K, Jia G J and Kelley A M 2008 Phytomass patterns across a temperature gradient of the North American Arctic tundra *J. Geophys. Res.* **113** 3–5
[87] Houghton R A, Hall F and Goetz S J 2009 Importance of biomass in the global carbon cycle *J. Geophys. Res.* **114** 1–13
[88] Epstein H E, Raynolds M K, Walker D A, Bhatt U S, Tucker C J and Pinzon J E 2012 Dynamics of aboveground phytomass of the circumpolar Arctic tundra during the past three decades *Environ. Res. Lett.* **7** 12
[89] Myers-Smith I H *et al* 2011 Shrub expansion in tundra ecosystems: dynamics, impacts and research priorities *Environ. Res. Lett.* **6** 045509
[90] Dorrepaal E 2007 Are plant growth-form-based classifications useful in predicting northern ecosystem carbon cycling feedbacks to climate change? *J. Ecol.* **95** 1167–80
[91] Thomson E R *et al* 2021 Multiscale mapping of plant functional groups and plant traits in the high Arctic using field spectroscopy, UAV imagery and sentinel-2A data *Environ. Res. Lett.* **16** 055006
[92] Tape K D, Hallinger M, Welker J M and Ruess R W 2012 Landscape heterogeneity of shrub expansion in Arctic Alaska *Ecosystems* **15** 711–24
[93] Leipe S C and Carey S K 2021 Rapid shrub expansion in a subarctic mountain basin revealed by repeat airborne LiDAR *Environ. Res. Commun.* **3** 071001
[94] Verbyla D 2008 The greening and browning of Alaska based on 1982–2003 satellite data *Glob. Ecol. Biogeogr.* **17** 547–55
[95] Gaglioti B V, Berner L T, Jones B M, Orndahl K M, Williams A P, Andreu-Hayles L, D'Arrigo R D, Goetz S J

and Mann D H 2021 Tussocks enduring or shrubs greening: alternate responses to changing fire regimes in the Noatak River Valley, Alaska *J. Geophys. Res.* **126** e2020JG006009
[96] Rocha A V, Loranty M M, Higuera P E, MacK M C, Hu F S, Jones B M, Breen A L, Rastetter E B, Goetz S J and Shaver G R 2012 The footprint of Alaskan tundra fires during the past half-century: implications for surface properties and radiative forcing *Environ. Res. Lett.* **7** 044039
[97] Bret-Harte M S, Mack M C, Shaver G R, Huebner D C, Johnston M, Mojica C A, Pizano C and Reiskind J A 2013 The response of Arctic vegetation and soils following an unusually severe tundra fire *Phil. Trans. R. Soc.* B **368** 20120490
[98] Racine C H, Johnson L A and Viereck L A 1987 Patterns of vegetation recovery after tundra fires in Northwestern Alaska *Arct. Antarct. Res.* **19** 461–9
[99] Beck P S A, Goetz S J, Mack M C, Alexander H D, Jin Y, Randerson J T and Loranty M M 2011 The impacts and implications of an intensifying fire regime on Alaskan boreal forest composition and albedo *Glob. Change Biol.* **17** 2853–66
[100] Johnstone J F, Rupp T S, Olson M and Verbyla D 2011 Modeling impacts of fire severity on successional trajectories and future fire behavior in Alaskan boreal forests *Landsc. Ecol.* **26** 487–500
[101] Johnstone J F, Kasischke E S, Johnstone J and Kasischke E 2005 Stand-level effects of soil burn severity on postfire regeneration in a recently burned black spruce forest 1 *Can. J. For. Res.* **35** 2151–63
[102] Mack M C, Treseder K K, Manies K L, Harden J W, Schuur E A G, Vogel J G, Randerson J T and Chapin F S 2008 Recovery of aboveground plant biomass and productivity after fire in mesic and dry black spruce forests of interior Alaska *Ecosystems* **11** 209–25
[103] Jandt R, Joly K, Randy Meyers C and Racine C 2008 Slow recovery of lichen on burned caribou winter range in Alaska tundra: potential influences of climate warming and other disturbance factors *Arct. Antarct. Alp. Res.* **40** 89–95
[104] Frost G V, Loehman R A, Saperstein L B, Macander M J, Nelson P R, Paradis D P and Natali S M 2020 Multi-decadal patterns of vegetation succession after tundra fire on the Yukon-Kuskokwim Delta, Alaska *Environ. Res. Lett.* **15** 025003
[105] Palm E C, Suitor M J, Joly K, Herriges J D, Kelly A P, Hervieux D, Russell K L, Bentzen T W, Larter N C and Hebblewhite M 2022 Increasing fire frequency and severity will increase habitat loss for a boreal forest indicator species *Ecol. Appl.* **32** e2549
[106] Wein R W and Bliss L C 1973 Changes in Arctic eriophorum tussock communities following fire *Ecology* **54** 845–52
[107] Hollingsworth T N, Johnstone J F, Bernhardt E L and Chapin F S 2013 Fire severity filters regeneration traits to shape community assembly in Alaska's Boreal Forest *PLoS One* **8** e56033
[108] Bernhardt E L, Hollingsworth T N and Chapin F S 2011 Fire severity mediates climate-driven shifts in understorey community composition of black spruce stands of interior Alaska *J. Veg. Sci.* **22** 32–44
[109] Wein R W and MacLean D A 1983 *The Role of Fire in Northern Circumpolar Ecosystems* ed R W Wein and D A MacLean (New York: Wiley) p 322